Design of an integrated optical source of twin photons

Ivan Avrutsky

Department of Electrical and Computer Engineering, Wayne State University, Detroit, Michigan 48202, USA

Alexander V. Sergienko

Department of Electrical & Computer Engineering and Department of Physics, Boston University, Boston, Massachusetts 02215, USA

The phase matching for the nonlinear process of frequency-degenerated spontaneous parametric downconversion in tunneling-coupled channel waveguides is analyzed. The use of type II nonlinear interaction with individual photons in each pair appearing in different output channels allows for constructing polarization entangled states for quantum information processing applications.

I. INTRODUCTION

Several novel areas of quantum-information processing including quantum cryptography, quantum teleportation, and linear-optical quantum computing have recently become a subject of intensive experimental research [1,2]. Sources of entangled photons based on bulk nonlinear crystals such as beta-barium borate (β-BBO) [3] have been widely used in early experiments. The development of robust, efficient, and compact sources of entangled photons has become a necessity for further progress in the area of applied quantum optics. While compact optical schemes [4] as well as micro-optical assemblies [5] and fiber-optical devices [6] are important milestones, only waveguide-based optical sources can eventually provide the desirable degree of dense integration, robustness, and stability.

Generation of entangled photons in optical waveguides has been experimentally verified recently [7–10]. Efficiency improvement of up to four orders of magnitude has been attributed to the waveguide geometry alone. We expect that the waveguide-based integrated optical source of entangled photons proposed in this paper will show similar efficiency improvement and will provide an acceptable level of entanglement fidelity. In the devices demonstrated so far, the pump photon and both generated entangled photons are guided in the same channel. It is vital for practical application to have an integrated optical source in which individual photons from each pair will appear in different output channels. Spatial separation of entangled photons resembles such in the noncollinear degenerated spontaneous parametric downconversion (SPDC) in nonlinear crystals, which is the most popular technique for generation of entangled states. The geometry of the nonlinear interaction in channel waveguides does not have to be noncollinear, though. The spatial separation can be achieved through precise engineering of modal indices in tunneling-coupled channel waveguides. The phase matching should be arranged so that downconverted photons cannot appear in the same output waveguide but instead must be directed to different outputs. The entanglement is achieved if photons of both polarizations can be guided in each of the output waveguides with equal probability so that the polarization in a given output

channel cannot be predicted in advance. The entangled photons in each pair will have different polarizations (type II nonlinear interaction).

In order to support a high efficiency of entangled-photon state production in a very compact volume of nonlinear interaction inside the integrated quantum logical unit, one has to be able to use a laser pump with a rather high power density. This requirement becomes even more critical in the case of using parametric downconversion in transverse pumping geometries [11,12]. This constraint practically rules out the use of such popular but optically soft material as lithium niobate. In this paper, we discuss the design principles of the tunneling-coupled channel waveguide source of entangled photons in a well-tested optically hard nonlinear material such as beta-barium borate (β-BBO) and we provide a practical design example based on He$^+$-ion implanted waveguides.

II. DESIGN PRINCIPLES

A. Phase matching conditions

The phase synchronism between the pump wave and downconverted waves is crucial for efficient generation of entangled photons. In bulk crystals, it can be achieved through compensation of chromatic dispersion by optical birefringence. Technically, this is realized through careful angular alignment and choice of the pump wave polarization. The phase-matching direction and polarizations of light waves are defined by linear optical properties, and thus they do not necessarily correspond to the direction and polarizations of the strongest nonlinearity. In addition, the wavelength range in which the angular alignment allows for achieving the phase synchronism is often limited as long as the spectral dispersion increases strongly for shorter optical wavelength while the birefringence is relatively constant over a wide spectral range.

In some materials, the additional degree of freedom is introduced by fabricating a volume grating, for example by periodic poling. Light diffraction at the grating of an appropriate period provides resonant phase velocity coupling between the waves that otherwise would be out of the phase
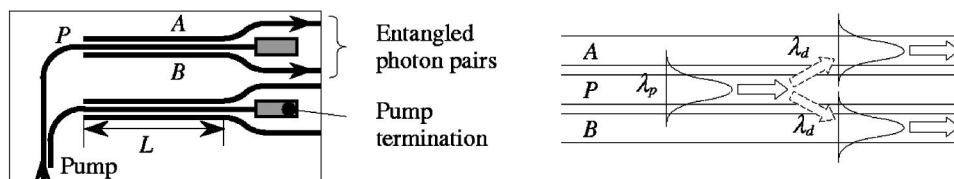
FIG. 1. Schematic structure of the proposed integrated optical source of polarization-entangled photons: the overall top view (left) and the tunneling-coupled channel waveguides section (right). The optical pump is delivered by the channel waveguide P. The down-converted polarization-entangled photons appear in the output channel waveguides A and B.

synchronism. Although quasi-phase-matching by diffraction at the volume grating introduces some decrease of the effective nonlinear coefficient (by a factor of $2/\pi$ for the periodically poled crystal with a perfectly adjusted period), the ability to choose any propagation direction and polarization allows us to benefit from using the strongest components of the nonlinear crystal's susceptibility tensor.

In integrated optical devices, light is confined to optical waveguides. To achieve the phase synchronism inside the waveguide, one can use optical anisotropy by routing waveguides along a suitable direction in a crystal. One can also use a quasi-phase-matching in waveguide gratings by combining the poling and waveguide creation processes. To achieve an effective diffraction coupling of guided modes in waveguides, the grating does not have to spread throughout the entire waveguide volume. Instead, it could be accomplished by a surface relief grating or by a grating fabricated in a thin layer positioned right on the top of the guiding layer. Finally, the waveguide geometry itself provides one more tool for the fine adjustment of phase velocities of the waves involved in nonlinear interactions. In fact, a spectral dispersion of guided modes can be used for phase matching even in the absence of optical birefringence and gratings. A representative example of an integrated optical device designed for efficient second-harmonic generation would be a GaAs/AlGaAs multilayer waveguide, in which phase synchronism is achieved between the pump photons coupled to the fundamental TE_0 and TM_0 modes at 1.55 μm and a double frequency photon guided by the TE_2 mode [13]. In a reciprocal process of parametric downconversion, a pump photon at 775 nm is expected to produce twin photons at 1.55 μm through a type II interaction so that the downconverted photons will have different polarizations. It is important to note that both GaAs and AlAs are optically isotropic crystals. Though their nonlinear second-order susceptibility is rather high ($d_{GaAs}=90$ pm/V), the angular phase synchronism is impossible. Fabrication of periodic structures for quasi-phase-matching in such material requires using rather complex technological operations such as wafer bonding or orientation-patterned epitaxial growth [14]. It is the guided mode dispersion which allows for a simple and elegant technical solution to achieve the phase matching in such a configuration. In another example of an in-waveguide generation of twin photons, the couterpropagating geometry is used [15,16]. The pump wave in this case is not guided, though. The incident angle of the pump wave is an adjustable parameter to achieve parametric fluorescence precisely degenerated in frequency. As long as the pump photons quickly leave the interaction region, the efficiency of downconversion is ex-

pected to be lower in such geometries compared to the case when all the waves are confined to waveguides. One peculiar advantage of the counterpropagating geometry is a substantial reduction of the spectral width of downconverted photons. This will help to improve the performance of entangled-photon quantum cryptography by minimizing the dispersion-induced pulse broadening in communication fiber links.

In this paper, we propose an alternative type of integrated optical device for efficient parametric downconversion and polarization-entangled two-photon state engineering. The innovative element of our design is in the combination of the nonlinear optical interaction inside a waveguide and light tunneling between closely routed waveguides. In the proposed device, pump photons are guided by channel P, and the downconverted photons appear in channels A and B (Fig. 1). The SPDC is combined with light tunneling from P to A and from P to B. Optical oscillations at the downconverted wavelength in P generate guided modes in A and B provided that proper phase-matching conditions are satisfied. In principle, only the waveguide P has to be nonlinear. In practice, it is convenient to fabricate all channel waveguides using the same material.

By physical nature, a set of tunneling-coupled modes in a system of closely routed channel waveguides is equivalent (but not identical) to a set of high-order modes in one complex waveguide that includes all the channels and the gaps between the channels [17]. From this point of view, the proposed structure can be considered as a particular case of modal phase matching. There are some technical differences in the mathematical description, though. It is known, for example, that in the case of two identical single-mode channel waveguides weakly coupled through tunneling, the set of modes of the complex waveguide contains a symmetric and an asymmetric mode (also called "supermodes" to distinguish them from the modes of the individual waveguides) with slightly different modal indices. The interference between the supermodes leads to periodic canceling of the electromagnetic field in one or another channel waveguide, which is treated as periodic transfer of optical power between the waveguides. In a sense, the supermodes never have identical modal indices due to the anticrossing effect, while the resonant light coupling certainly takes place between the identical waveguides. In other words, within the concept of supermodes, the resonant coupling between the waveguides takes place without exact matching of the supermodes' modal indices. This happens because none of the supermodes represents guided modes in any of the individual waveguides: only the combination of the supermodes does it.

Alternatively, a set of tunneling coupled modes in a system of two channel waveguides can be described using the coupled mode equations (also known as the approximation of slowly varying amplitudes). Perfect phase matching between the modal indices of individual waveguides is a necessary condition for effective resonant coupling. The descriptions based on the interference of the supermodes and on the coupled-modes equations are mathematically equivalent.

Compared to a single multimode waveguide similar to one described in [13], the proposed structure consisting of tunneling-coupled waveguides provides spatial separation of downconverted photons, while careful adjustment of modal indices leads to polarization entanglement. This is why we consider the tunneling-coupled waveguides as a new type of integrated optical device for generation of entangled photons.

The type II phase-matching condition in coupled waveguides can be written in terms of modal indices n,

$$\frac{1}{2}[n_M^A(2\lambda_p) + n_E^B(2\lambda_p)] = n^P(\lambda_p), \tag{1a}$$

$$\frac{1}{2}[n_E^A(2\lambda_p) + n_M^B(2\lambda_p)] = n^P(\lambda_p), \tag{1b}$$

where λ_p is the pump wavelength, subscripts E and M correspond to *TE* and *TM* polarizations, and superscripts A, B, and P indicate the waveguides. To ensure that both downconverted photons do not appear in the same output channel, the waveguides must be different. More precisely, their modal indices must be different enough so that the mismatches

$$\Delta n_A = \frac{1}{2}[n_E^A(2\lambda_p) + n_M^A(2\lambda_p)] - n^P(\lambda_p) \neq 0, \tag{2a}$$

$$\Delta n_B = \frac{1}{2}[n_E^B(2\lambda_p) + n_M^B(2\lambda_p)] - n^P(\lambda_p) \neq 0 \tag{2b}$$

will prevent efficient coupling of both downconverted photons to the same waveguide, either A or B. It is easy to check that once Eq. (1) is satisfied, the conditions (2a) and (2b) are essentially equivalent as long as the mismatches Δn_A and Δn_B in this case are different by sign only: $\Delta n_B = -\Delta n_A$. Note that if the waveguides A and B are identical, Eqs. (1) and (2) result in $\Delta n_A = \Delta n_B = 0$. It is also important to prevent the type I processes when both generated photons have the same polarization. The phase mismatches for the case when downconverted photons appear in different waveguides are as follows:

$$\Delta n_E = \frac{1}{2}[n_E^A(2\lambda_p) + n_E^B(2\lambda_p)] - n^P(\lambda_p) \neq 0, \tag{3a}$$

$$\Delta n_M = \frac{1}{2}[n_M^A(2\lambda_p) + n_M^B(2\lambda_p)] - n^P(\lambda_p) \neq 0. \tag{3b}$$

Using Eq. (1), one can find $\Delta n_E = [n_E^A(2\lambda_p) - n_M^A(2\lambda_p)]/2$ and $\Delta n_M = [n_M^A(2\lambda_p) - n_E^A(2\lambda_p)]/2 = -\Delta n_E$. The modal indices at

the downconverted wavelength can further be expressed through the mismatches Δn_A and Δn_E,

$$n_E^A(2\lambda_p) = n^P(\lambda_p) + \Delta n_A + \Delta n_E, \tag{4a}$$

$$n_M^A(2\lambda_p) = n^P(\lambda_p) + \Delta n_A - \Delta n_E, \tag{4b}$$

$$n_E^B(2\lambda_p) = n^P(\lambda_p) - \Delta n_A + \Delta n_E, \tag{4c}$$

$$n_M^B(2\lambda_p) = n^P(\lambda_p) - \Delta n_A - \Delta n_E. \tag{4d}$$

Finally, to prevent the type I process in which both photons appear in the same waveguide, one should require $n_E^A(2\lambda_p) \neq n^P(\lambda_p)$, $n_M^A(2\lambda_p) \neq n^P(\lambda_p)$, $n_E^B(2\lambda_p) \neq n^P(\lambda_p)$, and $n_M^B(2\lambda_p) \neq n^P(\lambda_p)$. This means $\Delta n_+ = \Delta n_A + \Delta n_E \neq 0$ and $\Delta n_- = \Delta n_A - \Delta n_E \neq 0$. Thus, in order to guarantee that the only efficient nonlinear process in the proposed waveguide structure is the type II downconversion in which the generated photons appear in different waveguides, one should satisfy the conditions (1) and make sure that the mismatches Δn_A, Δn_E, Δn_+, and Δn_- are large enough to prevent undesirable nonlinear interactions.

As a rule, any modification of a channel waveguide would affect both *TE* and *TM* modal indices. Thus it is not evident whether the conditions (1a) and (1b) can be simultaneously satisfied. Excluding $n^P(\lambda_p)$ from Eqs. (1a) and (1b), we obtain

$$n_E^A(2\lambda_p) - n_M^A(2\lambda_p) = n_E^B(2\lambda_p) - n_M^B(2\lambda_p). \tag{5}$$

The difference between the *TE* and *TM* modal indices is a nonmonotonic function of the waveguide thickness in a general case. In a symmetric isotropic planar waveguide, both modal indices approach cladding or core index for waveguide thickness t approaching zero or infinity, respectively (Fig. 2). Thus, one can find two different values of the waveguide thickness t (and/or width w for channel waveguides) such that Eq. (5) is perfectly satisfied. Further adjustment of the pump waveguide parameters will satisfy Eqs. (1a) and (1b) simultaneously.

The example with the symmetric isotropic waveguide is an idealistic abstraction as long as practically used nonlinear crystals are highly anisotropic and vertical structure of the planar waveguide is likely to be asymmetric. Nevertheless, it provides a useful insight into the properties of guided modes in planar waveguides and clearly indicates that condition Eq. (5) can potentially be satisfied for different waveguides A and B.

In the proposed concept, all necessary phase matchings and required mismatchings are provided by the waveguide design only. Thus the waveguide parameters no longer have much freedom to vary. Using of quasi-phase-matching may be helpful as long as it would allow for more flexibility in the waveguide design. As is described above, for a given thickness (or width) of the waveguide A, there is a unique value of the thickness of the waveguide B to satisfy Eq. (5), and further, there is a unique value of the thickness of the pump waveguide P to satisfy both Eqs. (1a) and (1b). These two requirements comprise two resonant conditions. The first one deals with the symmetry of the waveguides' indices and
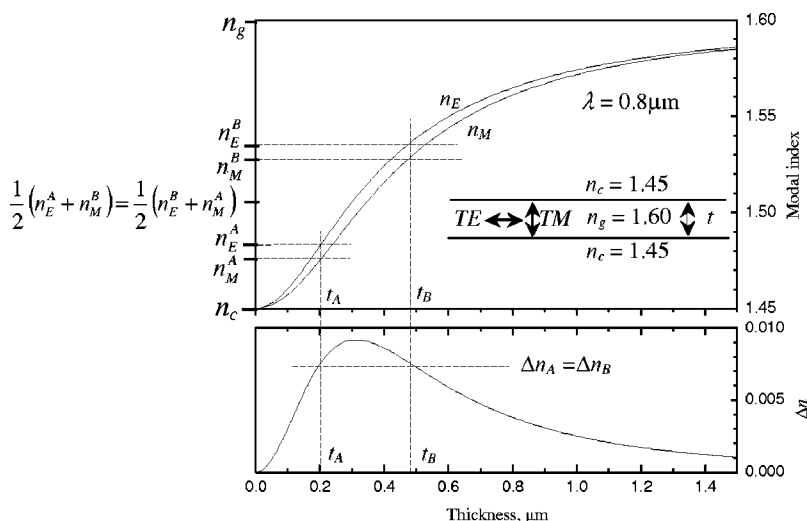
FIG. 2. Modal indices in a symmetric planar waveguide.

guarantees the polarization entanglement and spatial separation of the downconverted photons. If, for a given choice of the waveguides A and B, the left and right parts of Eq. (5) happen to be different, a periodic perturbation of the waveguides can be introduced to compensate for this mismatch. Such a technical solution, however, is not desirable because it may break the symmetry between the pairs of the entangled photons: for example, one pair (say, TE photon in A and TM photon in B) will be generated using the real phase matching, while the other pair (TM photon in A and TE photon in B) will be generated through the quasi-phase-matching process. As for the second resonant condition (adjustment of the pump waveguide thickness), there are no obvious side effects of using the quasi-phase-matching. A detailed analysis of quasi-phase-matching in a system of three channel waveguides (pump plus two spatially separated outputs) using, perhaps, superimposed gratings of different periods, is certainly a subject of a separate study.

B. Overlapping integrals

Three waves interact in the proposed structure: the pump wave at wavelength λ_p and the signal/idler waves at wavelength $2\lambda_p$. The efficiency of nonlinear interaction is thus proportional to the triple overlapping integral. The overlapping integrals for the processes described by the phase-matching conditions (1a) and (1b) are given by

$$\eta_{AM/BE} = \int \int E_M^A(2\lambda_p) E_E^B(2\lambda_p) E^P(\lambda_p) du dv, \qquad (6a)$$

$$\eta_{AE/BM} = \int \int E_E^A(2\lambda_p) E_M^B(2\lambda_p) E^P(\lambda_p) du dv, \qquad (6b)$$

where E is the strength of the electric field of the guided mode, superscripts A, B, and P indicate waveguides, subscripts E and M show mode polarization, and u and v are coordinates across the waveguide. Note that polarization of the pump mode has not been defined yet. It can be either TE or TM depending on the crystal orientation and structure of its nonlinearity tensor. As long as the phase-matching condi-

tions discussed above are satisfied and the overlapping integrals and appropriate components of the nonlinearity tensor are nonzero, downconversion is expected to take place. All mode fields in Eq. (6) are assumed to be normalized as follows:

$$\int \int |E|^2 du dv = 1, \qquad (7)$$

so that the overlapping integrals in Eq. (6) have dimensions of $1/\text{length}$ (say, cm^{-1}). To achieve the strongest entanglement, the overlapping integrals have to be identical. Only in this case is the polarization state of an individual photon in the output waveguide truly undetermined, and with equal probability it may become TE or TM. Expressions (6a) and (6b) are rather symmetric. At least in the case of strong confinement, the modal fields for TE and TM polarizations are almost identical, which results in similar values of the overlapping integrals. The overlapping integrals can be controlled by adjusting the gaps between the waveguides. This may, however, affect the modal indices. Rigorously speaking, optimization of the waveguide structure to achieve identical large values of the overlapping integrals must be done within the space of parameters that keep conditions (1) satisfied.

III. DESIGN EXAMPLE

A. Materials

The proposed device can be fabricated in a variety of materials. Waveguide fabrication technology is well-developed for lithium niobate (LiNbO_3). Periodically poled lithium niobate (PPLN) allows for quasi-phase-matching conditions achieved for practically any predetermined direction and polarization of the pump wave, including those corresponding to the strongest optical nonlinearity. While LiNbO_3 and PPLN are technologically the most developed materials for nonlinear integrated optics, they have low damage threshold and suffer from photorefraction, which makes the phase synchronism unstable. Barium borate (β-BBO) has been the material of choice for nonlinear optical applications as well as for generation of entangled-photon states in bulk
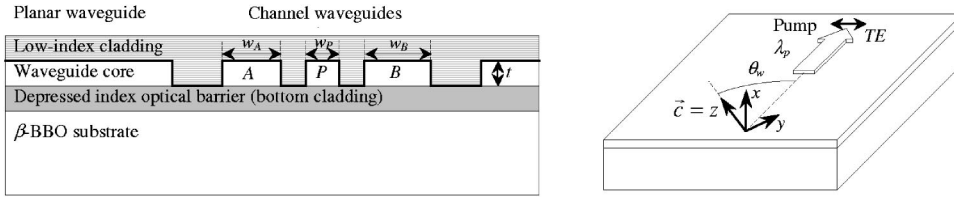
FIG. 3. Cross section of the waveguide structure (left) and schematic view of the crystal cut (right).

crystals. Its major advantages are high damage threshold and stability of the synchronism [18]. A further design example is given for β-BBO based waveguides.

Fabrication of planar waveguides in β-BBO is possible by high-energy He$^+$-ion implantation [19]. Light ions penetrate under the surface (up to 5 μm at an energy of 2 MeV), and only after losing energy to scattering with electrons do they start interacting with the crystal lattice, causing partial amorphization. The He-enriched layer has smaller refractive indices and thus forms the optical barrier (bottom cladding). To fabricate vertical barriers separating the channels, one can etch trenches between the waveguides and fill them with low-index material such as silica. The cross section of planar and channel waveguides is schematically shown in Fig. 3.

In order to realize the design principles described above, we first define the planar waveguide and the pump direction for collinear degenerated type II spontaneous parametric downconversion. Then, within the planar waveguide we define the channels A, B, and P and adjust their parameters to satisfy Eq. (1). In this example, we use approximate models based on the effective index method to describe anisotropic planar and channel waveguides.

For the crystal cut with the optical axis parallel to the waveguide plane, the extraordinary polarization of the pump corresponds to the TE polarization of the guided wave. The downconverted waves have both TE and TM polarizations.

For the pump (subscript p) and downconverted (subscript d) wavelengths ($\lambda_p = 400$ nm and $\lambda_d = 800$ nm), we calculated ordinary (subscript o) and extraordinary (subscript e) refractive indices of β-BBO using modified Sellmeier equations [20]: $n_{po} = 1.692\,932$, $n_{pe} = 1.567\,836$, $n_{do} = 1.660\,398$, and $n_{de} = 1.544\,261$. In the barrier, optical indices are smaller. Literature data on implantation-induced index changes are not very comprehensive. They are available only for the He-Ne laser wavelength of 632.8 nm and for a high implan-

tation dose that creates a large index step forming a multimode waveguide [21]. A smaller index step would be required for fabrication of single-mode waveguides. This can be achieved applying smaller implantation dose. It is reasonable to expect that the ordinary and extraordinary index steps in the barrier (subscript b) and in the guiding core (subscript g) would be changed proportionally. We accept the index steps to be $\Delta n_{ob} = -0.011$, $\Delta n_{eb} = -0.005$, $\Delta n_{og} = 0.0003$, and $\Delta n_{eg} = -0.0001$. With these index steps, a planar waveguide of thickness $t = 1.5$ μm will behave as a single-mode one for both pump and downconverted wavelengths. We assume that the cover layer as well as the material between the channel waveguides has an index of refraction slightly higher than that of fused silica: $n_c(\lambda) = n_{SiO_2}(\lambda) + 0.03$. Using the Sellmeier formulas for silica [22], the cladding index becomes $n_{cp} = 1.500\,127$ and $n_{cd} = 1.483\,321$ at the pump and downconverted wavelengths, respectively. Such cladding index adjustment brings the optimal width of the channel waveguides into the technologically comfortable range of single micrometers. Technically, a higher index can be achieved by doping silica with germanium oxide, as is done in conventional optical fibers. Another possibility would be to use silicon oxinitride by mixing silica with silicon nitride during deposition.

B. Waveguide structure

Let us consider a planar waveguide (Fig. 4 at the left). We assume that the optical axis is parallel to the plane of the waveguide.

For a given direction θ, refractive indices for electromagnetic waves polarized normally to the waveguide plane are equal to corresponding ordinary indices n_{ob} and n_{og}, while for the waves polarized parallel to the plane the refractive indices are calculated according to
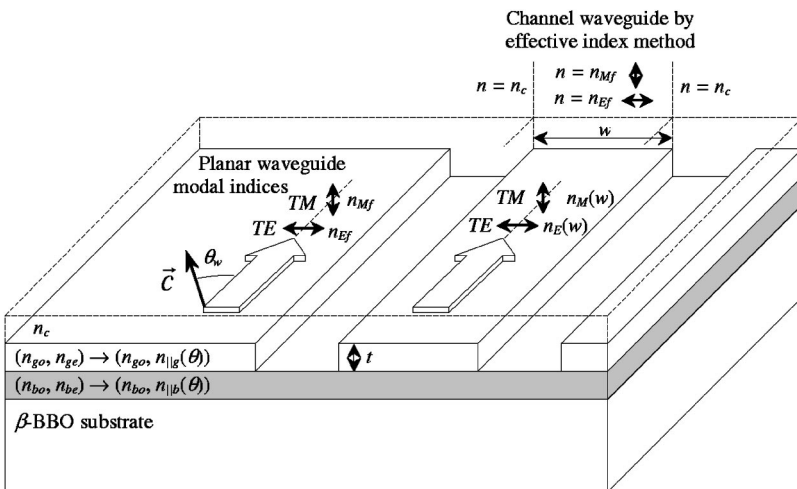

FIG. 4. Material and modal indices in the planar and channel waveguides.

$$n_{\parallel} = \frac{1}{\sqrt{\dfrac{\cos^2\theta}{(n_o)^2} + \dfrac{\sin^2\theta}{(n_e)^2}}}, \tag{8}$$

where n_o and n_e are wavelength-dependent ordinary and extraordinary indices of the materials (core or barrier). This formula is applied to the guiding layer and to the barrier (indices $n_{\parallel g}$ and $n_{\parallel b}$). In a simplified analysis of an anisotropic planar waveguide, we can use formulas for isotropic planar waveguides taking ordinary indices to estimate propagation constants for the *TM* modes, and $n_{\parallel}$ indices for the *TE* modes. Accurate but a lot more computation-extensive numerical methods are available for simulation of guided modes propagating in a planar waveguide at some angle with respect to the optical axis [23]. The built-in error in the simplified estimation is associated with longitudinal components of an electric field in the guided modes supported by the waveguide. For the weakly guiding structures, the error vanishes. In this approximation, the modal indices n_{Ef} and n_{Mf} for the fundamental *TE* and *TM* modes of the thin-film planar structure (subscript f) are implicitly defined by

$$\frac{2\pi}{\lambda}t\sqrt{n_{\parallel g}^2 - n_{Ef}^2} = \arctan\sqrt{\frac{n_{Ef}^2 - n_c^2}{n_{\parallel g}^2 - n_{Ef}^2}} + \arctan\sqrt{\frac{n_{Ef}^2 - n_{\parallel b}^2}{n_{\parallel g}^2 - n_{Ef}^2}}, \tag{9a}$$

$$\frac{2\pi}{\lambda}t\sqrt{n_{og}^2 - n_{Mf}^2} = \arctan\frac{n_{og}^2}{n_c^2}\sqrt{\frac{n_{Mf}^2 - n_c^2}{n_{og}^2 - n_{Mf}^2}}$$
$$+ \arctan\frac{n_{og}^2}{n_{ob}^2}\sqrt{\frac{n_{Mf}^2 - n_{ob}^2}{n_{og}^2 - n_{Mf}^2}}. \tag{9b}$$

Using Eqs. (8) and (9), the direction in which the phase-matching condition

$$\frac{1}{2}[n_{Mf}(2\lambda_p) + n_{Ef}(2\lambda_p)] = n_{Ef}(\lambda_p) \tag{10}$$

is satisfied for the modes in the planar waveguide is found to be $\theta_w \approx 46.1°$, a few degrees larger than in a bulk crystal $\theta_b \approx 42.4°$.

Now we use the effective index method [24] to estimate modal indices in channel waveguides as functions of the channel width w. The channel in the film is treated as an effective waveguide with vertical boundaries (Fig. 4). The claddings of the effective waveguide are symmetric and their index is n_c as defined previously. The core of the effective waveguide has indices n_{Ef} and n_{Mf} for the polarizations parallel and normal to the plane. Because the boundaries of the effective waveguide are normal to the plane of the film, the *TE* mode of the film becomes *TM* mode of the effective waveguide and vice versa. For clarity, we will keep the original definition of the polarization (the *TE* modes are polarized parallel to the plane of the film and the *TM* modes are polarized orthogonal to the plane), and make necessary corrections in the formulas for calculation of modal indices n_E and n_M in the effective waveguide,
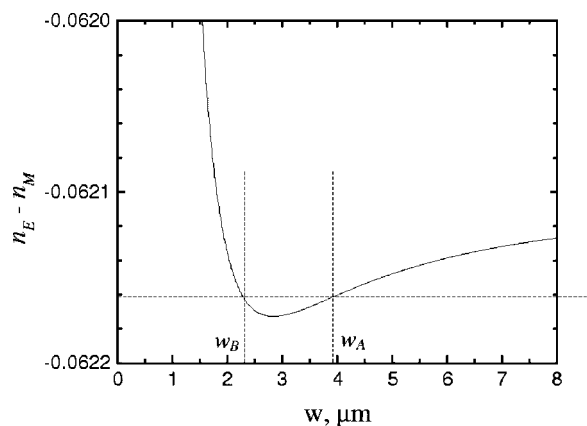

FIG. 5. Difference between the modal indices for *TE* and *TM* polarized modes as a function of the channel width.

$$\frac{2\pi}{\lambda}w\sqrt{n_{Ef}^2 - n_E^2} = 2\arctan\frac{n_{Ef}^2}{n_c^2}\sqrt{\frac{n_E^2 - n_c^2}{n_{Ef}^2 - n_E^2}}, \tag{11a}$$

$$\frac{2\pi}{\lambda}w\sqrt{n_{Mf}^2 - n_M^2} = 2\arctan\sqrt{\frac{n_M^2 - n_c^2}{n_{Mf}^2 - n_{EM}^2}}. \tag{11b}$$

When the channel width approaches zero, $w \to 0$, the guided mode is mainly localized in the cladding with a vanishing low fraction of optical power propagating in the core. The modal index, consequently, approaches the cladding index: $n_E \to n_c$ and $n_M \to n_c$. When the channel width becomes large, the guided mode is localized mainly in the core, so that the modal indices approach the film indices: $n_E \to n_{Ef}$ and $n_M \to n_{Mf}$ for *TE* and *TM* polarizations respectively. Particular ways how the modal indices are varying with the channel width depend in part on the polarization of light as long as the boundary conditions are polarization-sensitive. All these peculiarities are described by Eqs. (11a) and (11b).

At the downconverted wavelength, the difference $\Delta n(w, \lambda_d) = n_E(w, \lambda_d) - n_M(w, \lambda_d)$ reaches a negative minimum at $w \approx 2.8$ μm (Fig. 5). We pick up two values w_A and w_B left and right from the minimum such that $\Delta n(w_A, \lambda_d) = \Delta n(w_B, \lambda_d)$, which will automatically satisfy Eq. (5). An example of such a pair would be $w_A = 3.9$ μm and $w_B = 2.3$ μm. Modal indices for the channel waveguides A and B become the following: $n_E^A = n_E(w_A, \lambda_d) = 1.587\,624$, $n_M^A = n_M(w_A, \lambda_d) = 1.649\,786$, $n_E^B = n_E(w_B, \lambda_d) = 1.583\,409$, and $n_M^B = n_M(w_B, \lambda_d) = 1.645\,570$. Note that due to the choice of w_A and w_B, the following holds: $(n_M^A + n_E^B)/2 = (n_E^A + n_M^B)/2 = 1.616\,597$, and this must be the modal index $n_E^P(\lambda_p)$ of the pump wave. Using Eq. (11a), the appropriate width of the pump waveguide is found to be $w_P \approx 1.422$ μm. This concludes the design of the waveguides. Gaps between the waveguides should be small enough to provide tunneling coupling. Optimal coupling strength and thus the gap size would depend on the waveguide length.

To illustrate the modal fields and estimate the overlapping integrals in this numerical example, we have chosen the gaps to be 0.2 μm (between A and P) and 0.3 μm (between P and B). As long as the waveguides A and B are different, these
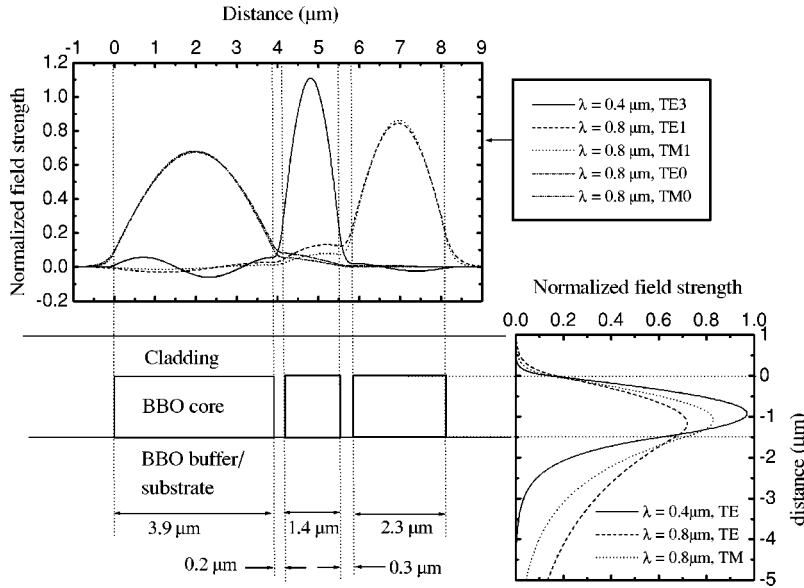
FIG. 6. The modal fields in a thin-film waveguide (bottom right), the in-plane modal fields calculated using the effective index method (top), and the cross section of the waveguide structure scaled to fit the distance axes of the graphs representing the modal fields (bottom left).

gaps must also be different to provide similar values of the overlapping integrals (6a) and (6b). No careful adjustment has been done, though. Figure 6 at the bottom right shows the mode profiles for the thin-film waveguides. A graph at the top shows the in-plane modes calculated in accordance with the effective index method. The bottom-left drawing shows schematically the waveguide structure cross section scaled to fit the distance axes of the graphs. With modal fields calculated as described above, the triple overlapping integrals become $\eta_{AM/BE}=38$ cm^{-1} and $\eta_{AE/BM}=34$ cm^{-1}. Most of contribution to the overlapping integrals comes from the area of the waveguide P, while contribution from the areas of waveguides A and B vanishes due to the oscillating nature of the modal fields. The difference between the overlapping integrals is less than 12%, thus one may expect high-fidelity generation of polarization-entangled photons separated to the outputs A and B.

Phase-matching conditions (1) are satisfied so that efficient downconversion is expected to generate photons of different polarizations in the output waveguides A and B. The phase mismatches for other (undesirable) nonlinear interactions are as follows: $|\Delta n_A|=|\Delta n_B|=0.002\,108$, $|\Delta n_E|=|\Delta n_M|=0.031\,081$, $|\Delta n_+|=0.028\,973$, and $|\Delta n_-|=0.033\,189$. The smallest mismatch corresponds to the case when photons of different polarizations appear in the same waveguide. When interaction length L is considerably larger than $\lambda_p/(n_E^P|\Delta_A|) \approx 117$ μm, the mismatch will effectively prevent downconverted photons from entering the same waveguide.

The above simulations show that the required relationship between the modal indices is feasible. More accurate simulation tools such as the vector beam propagation method or various finite-element methods can be used for precise design. This, however, would be an academic rather than practically important exercise as long as the key material parameters such as indices of refraction in the ion-implanted area are known with limited accuracy. For practical realization of the proposed source, it seems reasonable to rely on the choice of the angle θ and the bottom barrier design as described above. The final adjustment of modal indices is then achieved by varying the channels' widths. Thus, precise measurements of modal indices in channel waveguides of different width at both pump and downconverted wavelengths would be required. This could be done, for example, by fabricating a weak Bragg grating over the channel waveguide and measuring the Bragg wavelength [25], or by measuring the in-plane angle of light tunnel-coupled from a cannel waveguide to a planar waveguide [26]. Based on the measured data, one would be able to choose the widths of the channel waveguides for final implementation. In addition, barium borate is an electro-optic crystal and thus the fine adjustment of modal indices could be achieved by applying a dc voltage to control electrodes.

C. Crystal orientation

In a uniaxial crystal, optical indices are defined by the angle between the optical axis and the direction of propagation and by the light wave polarization. For the waveguide design described above, it is essential to keep the optical axis parallel to the substrate surface. Directions of other crystal axes may seem to be not important. Indeed, for analysis of phase-matching conditions, it does not matter if the crystal has an x-cut or a y-cut, because linear optical indices have axial symmetry with respect to the z axis. On the contrary, for the nonlinear optical interactions, the orientations of all three crystal's axes are important because the tensor of nonlinear optical coefficients has lower symmetry compared to the ellipsoid of linear optical indices.

In the xyz coordinates of the crystal lattice (z is parallel to the optical axis), the direction of the pump beam is characterized by the polar angle θ with respect to z and the azimuth angle φ with respect to x (Fig. 7, left). The effective nonlinear coefficient for type II parametric downconversion in a rhombohedral space group $3m$ crystal is given by [27,28]

$$d_{eff11} = d_{22} \cos(3\varphi)\cos^2 \theta, \qquad (12)$$

where d_{22} is the primary (the largest) nonlinear coefficient. Equation (12) defines azimuth angles φ corresponding to the
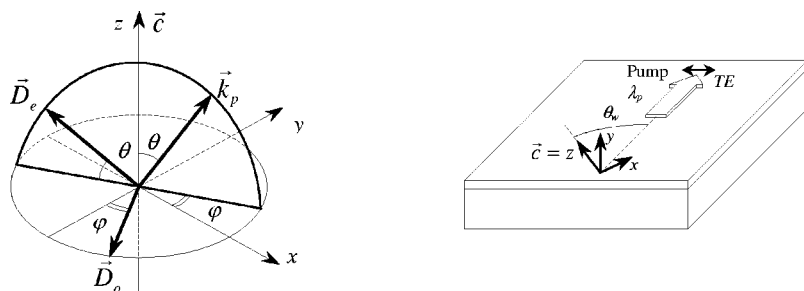
FIG. 7. Polar and azimuth angles that define effective nonlinearity of the BBO crystal (left) and schematic view of the crystal cut suitable for the proposed integrated optical source of entangled photons (right).

maxima of the magnitude of effective nonlinearity: $\varphi=0°$, 60°, and 120° with respect to the x axis. In particular, a favorable configuration is realized with the pumping beam propagating in the zx plane ($\varphi=0°$). The extraordinary polarization of the pump beam in this case corresponds to the electric flux density vector $\vec{D}_e$ being parallel to the zx plane. In contrast, if the pumping beam propagates in the zy plane, the effective nonlinearity vanishes so that even with the phase-matching conditions perfectly satisfied, there will be no downconversion.

We must note that in the technical literature on BBO there is some discrepancy as to the definition of crystal axes x and y. Some vendors of BBO crystals provide a different formula for effective nonlinearity: $d_{eff11}=[d_{11}\sin(3\varphi)+d_{22}\cos(3\varphi)]\cos^2\theta$, with d_{11} being the major nonlinear term ($d_{11}\gg d_{22}$). In such a case, the conclusions about the efficiency of downconversion for the pumping beams propagating in the zy and zx planes have to be switched to the opposite.

IV. CONCLUSION

We propose an integrated optical source of entangled photons based on type II degenerated spontaneous parametric downconversion in tunneling-coupled channel waveguides. This device can form a base for designing integrated linear-optical quantum logic circuits.

ACKNOWLEDGMENTS

[1] *The Physics of Quantum Information: Quantum Cryptography, Quantum Teleportation, Quantum Computation*, edited by D. Bouwmeester, A. Ekert, and A. Zeilinger (Springer, Berlin, 2000).

[2] G. Jaeger and A. V. Sergienko, *Multi-photon Quantum Interferometry*, in *Progress in Optics*, edited by E. Wolf (Elsevier Science, Amsterdam, 2001), Vol. 42.

[3] P. Kwiat, H. Weinfurter, H. Herzog, A. Zeilinger, and M. A. Kasevich, Phys. Rev. Lett. **74**, 4763 (1995).

[4] J. Brendel, N. Gisin, W. Tittel, and H. Zbinden, Phys. Rev. Lett. **82**, 2594 (1999).

[5] J. Volz, C. Kurtsiefer, and H. Weinfurter, Appl. Phys. Lett. **79**, 869 (2001).

[6] M. Fiorentino, J. E. Sharping, P. Kumar, A. Porzio, and R. S. Windeler, Opt. Lett. **27**, 649 (2002).

[7] K. Banaszek, A. B. U'Ren, and I. A. Walmsley, Opt. Lett. **26**, 1367 (2001).

[8] S. Tanzilli, W. Tittel, H. De Riedmatten, H. Zbinden, P. Baldi, M. De Micheli, D. B. Ostrowsky, and N. Gisin, Eur. Phys. J. D **18**, 155 (2002).

[9] A. Yoshizawa, R. Kaji, and H. Tsuchida, Electron. Lett. **39**, 621 (2003).

[10] K. Sanaka, K. Kawahara, and T. Kuga, Phys. Rev. Lett. **86**, 5620 (2001).

[11] Z. D. Walton, M. C. Booth, A. V. Sergienko, B. E. A. Saleh, and M. C. Teich, Phys. Rev. A **67**, 053810 (2003).

[12] Z. D. Walton, A. V. Sergienko, B. E. A. Saleh, and M. C. Teich, Phys. Rev. A **70**, 052317 (2004).

[13] S. Ducci, L. Lanco, V. Berger, A. De Rossi, V. Ortiz, and M. Calligaro, Appl. Phys. Lett. **84**, 2974 (2004).

[14] K. L. Vodopyanov, O. Levi, P. S. Kuo, T. J. Pinguet, J. S. Harris, M. M. Fejer, B. Gerard, L. Becouarn, and E. Lallier, Opt. Lett. **29**, 1912 (2004).

[15] M. C. Booth, M. Atature, G. Di Giuseppe, B. E. A. Saleh, A. V. Sergienko, and M. C. Teich, Phys. Rev. A **66**, 023815 (2002).

[16] A. De Rossi and V. Berger, Phys. Rev. Lett. **88**, 043901 (2002).

[17] *Guided-Wave Optoelectronics*, edited by T. Tamir (Springer, New York, 1988).

[18] P. Becker, Adv. Mater. (Weinheim, Ger.) **10**, 979 (1998).

[19] A. Boudrioua, P. Moretti, J. C. Loulergue, and K. Polgar, Opt. Mater. (Amsterdam, Neth.) **14**, 31 (2000).

[20] D. Zhang, Y. Kong, and J. Zhang, Opt. Commun. **184**, 485 (2000).

[21] C. Bakhouya, A. Boudrioua, R. Kremer, P. Moretti, J. C. Loulergue, and K. Polgar, Opt. Mater. (Amsterdam, Neth.) **18**, 73 (2001).

[22] *Handbook of Optical Constants of Solids*, edited by E. D. Palik (Academic, New York, 1991).

[23] I. Avrutsky, J. Opt. Soc. Am. A **20**, 548 (2003).

[24] M. Adams, *An Introduction to Optical Waveguides* (Wiley,

New York, 1981).

[25] S. Pissadakis, L. Reekie, M. Hempstead, M. N. Zervas, and J. S. Wilkinson, Appl. Surf. Sci. **153**, 200 (2000).

[26] D. V. Svistunov, J. Opt. A, Pure Appl. Opt. **6**, 859 (2004).

[27] R. W. Boyd, *Nonlinear Optics*, 2nd ed. (Academic Press, New York, 2003).

[28] R. S. Klein, G. E. Kugel, A. Maillard, A. Sifi, and K. Polgar, Opt. Mater. (Amsterdam, Neth.) **22**, 163 (2003).